There is no single functional atlas even for a single individual: Parcellation of the human brain is state dependent

Mehraveh Salehi*[1,2], Abigail S. Greene[3], Amin Karbasi[1,2], Xilin Shen[5], Dustin Scheinost[4,5], R. Todd Constable[3,5,6]

Departments of:

[1]Electrical Engineering, Yale University
[2]Yale Institute for Network Science (YINS), Yale University
[3]Interdepartmental Neuroscience Program, Yale University
[4]Statistics, Yale University
[5]Radiology and Biomedical Imaging, Yale School of Medicine
[6]Neurosurgery, Yale School of Medicine

Submitted to: BioRxiv, October 1, 2018

Address Correspondence to:

Mehraveh Salehi
Department of Electrical Engineering, Yale University
Yale MRRC, The Anlyan Center
300 Cedar Street
New Haven, CT 06520
USA
Email: mehraveh.salehi@yale.edu
Phone: (203) 535-8674

Key words: functional brain atlas; state-specific parcellation; task decoding; behavior prediction; functional connectivity; fMRI

Abstract

The goal of human brain mapping has long been to delineate the functional subunits in the brain and elucidate the functional role of each of these brain regions. Recent work has focused on whole-brain parcellation of functional Magnetic Resonance Imaging (fMRI) data to identify these subunits and create a functional atlas. Functional connectivity approaches to understand the brain at the network level, require such an atlas to assess connections between nodes and extract network properties. While no single functional atlas has emerged as the dominant atlas to date, there remains an underlying assumption that such an atlas exists. Using fMRI data from a highly sampled subject as well as two independent replication data sets, we demonstrate that functional atlases reconfigure substantially and in a meaningful manner, according to brain state.

Introduction

The field of human brain mapping, as the name suggests, has the goal of assigning functions to brain regions. To understand how the brain works, it is first necessary to define the minimal functional units in the brain at the macroscopic level considered in neuroimaging. These subunits are called a variety of terms, including nodes, parcels, cortical areas, or regions of interest (ROIs); while different analysis traditions favor different terms, each describes the same fundamental building block of macroscale neural circuitry: a spatially contiguous region of the human brain that is homogeneous and distinct in its functional identity. Individual areas may have unique combinations of cells and microstructure, but the overarching feature of interest is their function, and their functional architecture reflecting their connections to other brain regions. There has been no consensus to date, however, as to how to best define this underlying atlas, consisting of these functionally distinct, spatially contiguous nodes.

Since the early cytoarchitectonic atlas of Brodmann[1], there have been numerous attempts at subdividing the brain into small anatomical or functional subunits and assigning roles to these brain regions[2-7]. Neuroimaging-based parcellation approaches are attractive because they allow whole-brain parcellations in individuals[8-11] or groups of subjects[12-18] (for a review see Eickhoff et al.[19]). Most recent neuroimaging-based parcellation algorithms have been based entirely on functional connectivity data[12-15] or combinations of anatomical and functional data[16,17]. In addition, meta-analytic databases such as BrainMap[20] and NeuroSynth[21] have attempted to collate information from thousands of studies to assign functional identities to brain regions, and clustering methods have been developed to translate these findings into nodes[22]. Yet all of these commonly adopted parcellations, whether at the individual- or group-level, define a single functional atlas for all different brain states, assuming that nodes are homogenous in function with no state-dependent variability in size, shape or position.

Here, we challenge the fundamental assumption that a single functional atlas exists. We demonstrate that node boundaries change substantially across task conditions, yet are reliably reproducible within a condition. We provide evidence that node configuration can provide meaningful information on brain state. We do so by showing that a measure of node configuration as coarse as node size can significantly predict the task condition under which the data was acquired, for novel runs of a left-out subject, as well as the within-condition task performance for a left-out session in the same subject. These results have major implications for neuroscience both in terms of how we interpret previous findings, and in terms of re-adjusting how we think about the goals of human brain mapping.

Results

Three independent data sets are used to support these findings. In the first, 30 sessions of fMRI data were obtained from a single subject; each session was approximately 60 minutes long and included 6 task conditions (*n*-back[23], gradual-onset continuous performance task [gradCPT][24-26]. , stop-signal [SST][27], card guessing[28], Reading the Mind in the Eyes[29], and movie watching) and 2 rest conditions. Data were acquired from a single subject to eliminate the confound of inter-individual variations in anatomy, which would contribute to the variance in node boundaries[30]. The high number of fMRI sessions acquired in a single subject allows us to demonstrate consistent within-condition parcellations across sessions, while also demonstrating significantly different cross-condition parcellations. Since a single subject was used, the null hypothesis would be consistent parcellations across all sessions and conditions. A second, independent data set was used from Midnight Scan Club (MSC)[31], to replicate these findings and demonstrate their generalizability. This publicly available data set consists of a set of 8 individuals scanned, under both resting-state and task conditions, 10 times (10 sessions) each. Finally, rather than measuring consistency within a subject across sessions, we used the Human Connectome Project (HCP)[32] data (n=514) to demonstrate that even when collapsing across subjects (rather than sessions), we observe that different conditions lead to reproducibly different functional parcellations.

In the first data set, we applied an extended version of our recently developed individualized parcellation algorithm[10] to each functional run, generating one parcellation atlas for each condition and each scanning session (8 conditions × 30 sessions = 240 atlases total). By taking the majority vote over all sessions of each condition, we generated condition-specific parcellations. Figure 1a visualizes these parcellations using a force-directed graph (see Methods). Nodes are colored by the magnitude of reconfiguration in the given condition relative to Rest 1, demonstrating that nodes with high reconfiguration are broadly distributed and condition-specific. Increased similarity of reconfiguration maps is observed (Figure 1a) among condition-specific parcellations with increased pairwise similarity (Figure 1b). Consistent with our expectations, Rest 1 and Rest 2 parcellations are highly similar to each other, while the parcellation for the movie-watching condition is the most distinct (Figure 1).

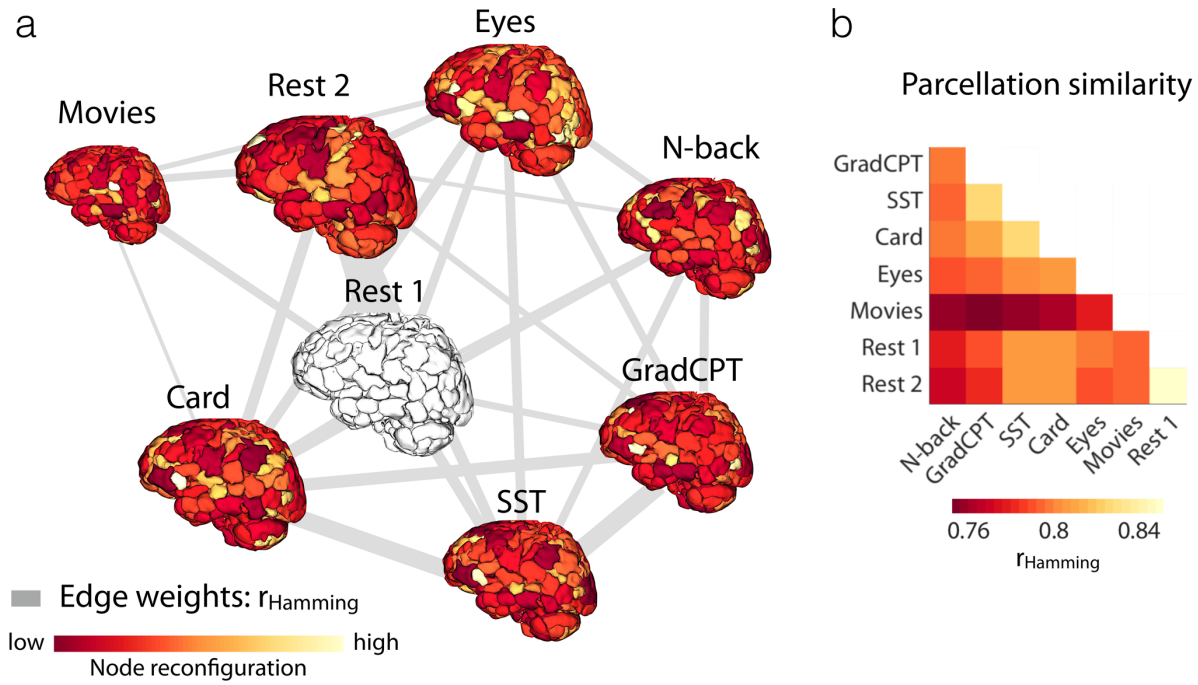

Figure 1. Visualization of the condition-specific functional atlases. (a) Condition-specific functional atlases are visualized in a force-directed graph, with edge weights indicating the similarity between parcellations, measured by $r_{Hamming}$ = 1-Hamming distance relative to the atlas from the 1st resting-state acquisition. Force-directed graphs attempt to visually organize networks such that the energy of the graph as a whole is minimized. This is accomplished by assigning both repulsive and attractive forces to each pair of nodes such that the nodes with stronger interconnections are displayed closer to each other and the ones with weaker connections are more distant. Brain size is proportional to the graph theory measure degree. Edge thickness is proportional to the edge weights. Nodes are colored by the magnitude of reconfiguration in the given condition relative to Rest 1. (b) Cross-condition parcellation similarity measured by $r_{Hamming}$.

To quantitatively examine these parcellation changes across conditions, we applied a voting-based ensemble method, randomly dividing all sessions for a given condition into two equal-sized groups, obtaining the majority-vote over each group, and computing the similarity between pairs of parcellations (see Methods). This was done both within and across functional conditions. We repeated this analysis 1000 times, generating 1000 pairwise similarity matrices. Parcellation similarity was considered at two scales: at the fine scale, we assessed the fraction of voxels that retained their node assignment (Figure 2a, d); at the coarse scale, we computed the rank correlation between node-size vectors (Figure 2b, e) for all condition pairs. The results demonstrate that parcellations are significantly more similar within each functional condition than across different conditions (KS-test; $p<0.001$). This finding also holds true when node size is considered as a means to summarize atlas boundaries (KS-test; $p<0.001$). The primary finding is that parcellations are highly reproducible within a functional condition, and rearrange significantly between conditions. These changes are reflected even in a coarse-scale feature of spatial topography, i.e. node-size.

Next, we demonstrate that the observed task-evoked parcellation reconfiguration is consistent across sessions and specific to each condition. To this end, we built a fully cross-validated predictive model that predicts the functional condition under which novel runs were acquired, based solely on the node size vector. Prediction accuracies—measured as precision and recall for each condition—were significantly higher than random for all conditions (mean accuracy = 71%; Figure 2c). That a measure of spatial topography as coarse as node size can significantly predict which task a subject is performing suggests that functional brain atlases reconfigure with task (in this case a proxy for brain state) in a consistent manner, forming a generalizable and robust signature of brain organization during that condition. Successful prediction also demonstrates that cross-condition reconfigurations are not driven by noise.

While the overall stability of the functional atlases within each condition was high, subtle variations were observed across different sessions of the same condition. To examine if node reconfigurations contain meaningful within-session information, we attempted to predict task performance using node-size as the model feature. Task performance was used as a proxy for level of engagement in the task, reflecting more fine-grained variations in brain state than can be captured by simply considering task state (see Methods for details of the behavioral measures that were used for each task). To this end, a linear regression model was employed in a leave-one-out cross-validated framework (see Methods for details), for each task independently. We used coefficient of determination (r-value) to assess the predictive power of the model. Task performances were successfully predicted from node sizes (Figure 2f), indicating that node reconfigurations from session to session, within a task condition, reflect meaningful changes in brain function. The success of these predictions again rules out the possibility that even session-to-session node reconfigurations are simply driven by noise.

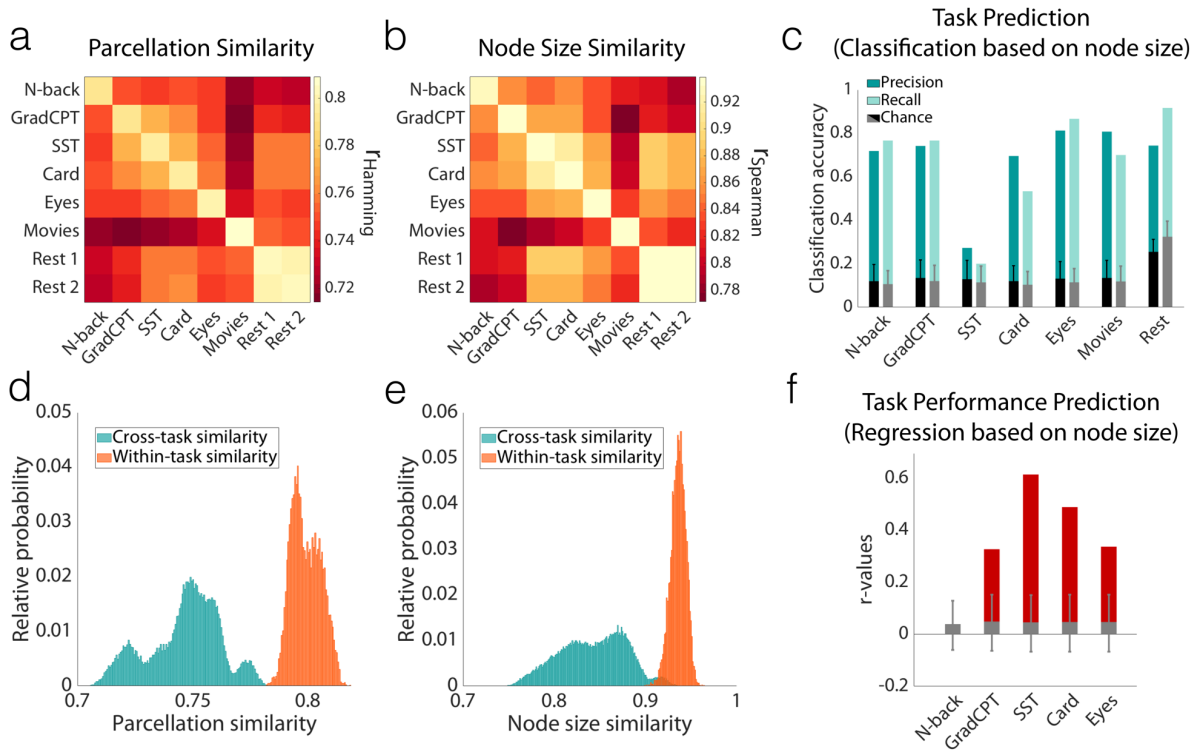

Figure 2. Node definitions change with task condition; Yale single-subject data. a) Pairwise parcellation similarity was calculated within and across functional conditions (8 conditions, N=30 sessions), using voting-based ensemble analysis with 1000 iterations. The matrix represents the average over all iterations. Similarity was assessed by $r_{Hamming}$ =1-Hamming distance. b) The same analysis as (a) was performed, this time using rank correlation of node-size vectors ($r_{Spearman}$) as a proxy for parcellation similarities. c) The bars report the accuracy of predicting the functional condition using a leave-one-out cross-validated GBM classifier with node sizes as features. The predictive power is measured by precision (dark cyan) and recall (light cyan) values for each condition. The precision (black) and recall (gray) values of 1000 null models are also reported (error bars represent ±s.d.). d) A histogram of the parcellation similarities for all 1000 iterations is depicted for within-condition (diagonal elements in [a]) and cross-condition (off-diagonal elements in [a]) comparisons. The two distributions are significantly different (KS-test; $p<0.001$). e) A histogram of the node size similarities for all 1000 iterations is depicted for within-condition (diagonal elements in [b]) and cross-condition (off-diagonal elements in [b]) comparisons. The two distributions are significantly different (KS-test; $p<0.001$). f) The bars report the accuracy of predicting task performance using a leave-one-out cross-validated linear regression model with node sizes as features. Predictive power is measured by square root of coefficient of determination (r-value).

Replication of the state-evoked atlas reconfiguration across data sets

We replicated our main findings by leveraging a publicly available data set: Midnight Scan Club (MSC)[31]. The MSC data are particularly well suited for this analysis, as they include task-based and resting-state fMRI data from 10 individuals, each of whom was scanned 10 times. Each scan session included seven runs of tasks (semantic-coherence [2 runs], memory [scenes, faces, and words; each 1 run], and motor [2 runs] tasks) and 1 resting-state run (eyes open). Two individuals were excluded from the analyses, one (MSC10) due to missing data and the other (MSC08) due to excessive head motion (see Methods for details), leaving 8 individuals (4 females; age = 24-34) for analysis.

For each individual, we repeated the voting-based ensemble analysis described above and calculated the similarity between each task- (or rest-) based pair of parcellations. Figure 3 demonstrates the pairwise parcellation similarities, averaged over individuals (Figure 3a,d: fine-scale similarity; Figure 3b,e: coarse-scale similarity). Figure S1 shows the similarity matrices of each individual separately. Confirming the finding from the single subject data described above, we observed that functional atlases are significantly more similar within condition than across conditions (KS-test, $p<0.001$). Similarly, node sizes are significantly more similar within a condition (KS-test, $p<0.001$). Predictive modeling based on node size could significantly predict condition for a novel run (mean accuracy = 66%; Figure 3c) and generalized across individuals. That all the predictions were successful, despite the additional variance introduced by inter-individual anatomical variations, is a strong indication of the functional significance of task-evoked node reconfigurations. The findings from this independent data set replicate the single subject findings.

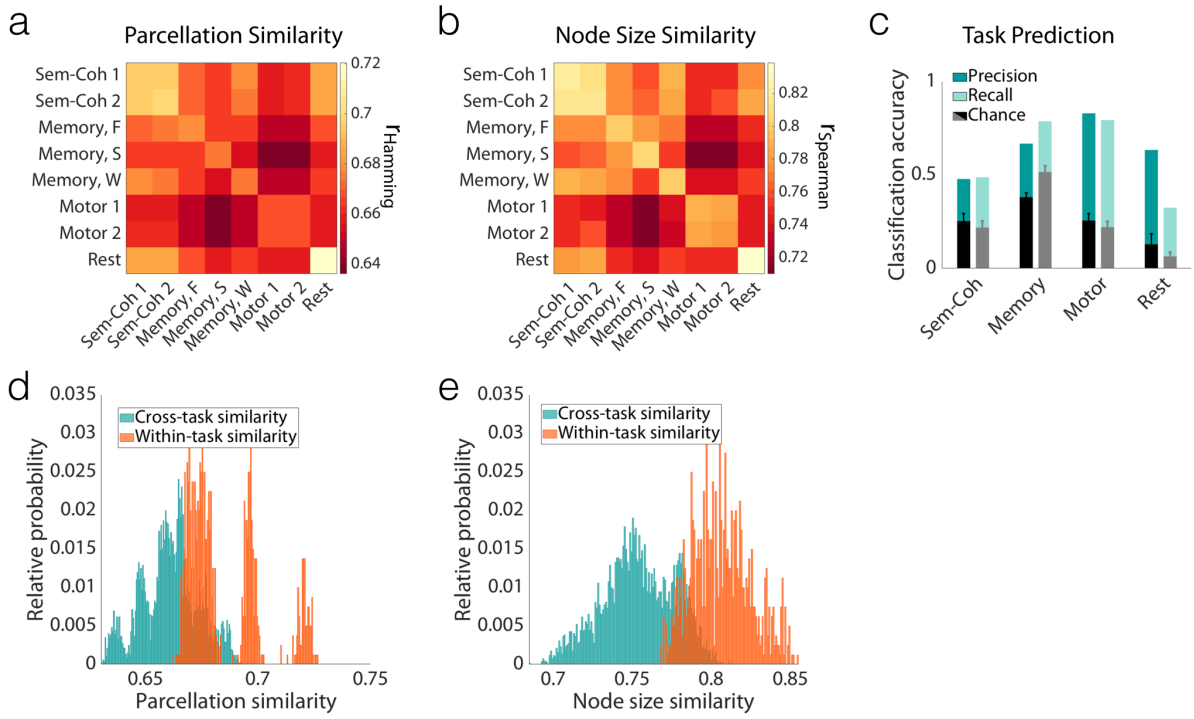

Figure 3. Replication of the finding that node definitions change with task condition; Midnight Scan Club (MSC) data. a) Pair-wise parcellation similarity was calculated within and across functional conditions, averaged over all individuals. For every individual, voting-based ensemble analysis was used with 100 iterations. The matrix represents the average over all iterations. Similarity was assessed by $r_{Hamming}$ =1-Hamming distance. b) The same analysis as (a) was performed, this time using rank correlation of node-size vectors ($r_{Spearman}$) as a proxy for parcellation similarities. c) The bars report the accuracy of predicting the functional condition using a leave-one-out cross-validated GBM classifier with node sizes as features. The predictive power is measured by the precision (dark cyan) and recall (light cyan) values for each condition. The precision (black) and recall (gray) values of 1000 null models are also reported (error bars represent ±s.d.). d) A histogram of parcellation similarities for all 100 iterations (averaged over all individuals) is depicted for within-condition (diagonal elements in [a]) and cross-condition (off-diagonal elements in [a]) comparisons. The two distributions are significantly different (KS-test; $p<0.001$). e) A histogram of node size similarities for all 100 iterations (averaged over individuals) is depicted for within-condition (diagonal elements in [b]) and cross-condition (off-diagonal elements in [b]) comparisons. The two distributions are significantly different (KS-test; $p<0.001$).

The results from the previous two data sets relied upon the construction of individual atlases across both sessions and conditions and were evaluated in terms of how the atlas *within an individual* changed between conditions. Next, we used the Human Connectome Project (HCP)[33] data to determine if such condition-dependent reconfigurations could be observed when collapsing across multiple subjects. The HCP data set includes task-based and resting-state fMRI data from 514 individuals (284 females; age = 22-36+), each of whom was scanned over a period of two days. Each scan session included seven tasks (day 1: working memory (WM), gambling, and motor tasks; day 2: language, social, relational, and emotion tasks) and 2 resting-states (one on each day).

We repeated the voting-based ensemble analysis described above, this time replacing sessions with subjects such that, for a given condition, we randomly divided all subjects into two equal-sized groups, obtained the majority-vote over each group, and computed the similarity between pairs of parcellations (see Methods). We repeated this analysis 1000 times. Figure 4 demonstrates the pairwise parcellation similarities across subjects. Despite the introduction of inter-individual anatomic and functional organization variance, the primary finding that the parcellation map changes with condition remains highly significant (Figure 4a,d: fine-scale similarity [KS-test, $p<0.001$]; Figure 3b,e: coarse-scale similarity [KS-test, $p<0.001$]). As an even stronger assessment of generalizability, we repeated our prediction analysis to predict the functional condition of data from previously unseen subjects based on node size. Given that we had a larger sample size (n=514), we further challenged our model by employing a 10-fold cross-validated pipeline (rather than leave-one-out). We observed that our model can significantly predict functional condition in novel subjects (mean accuracy = 73%; Figure 4c). This observation demonstrates an even stronger replication of our main findings; that is, the observed state-evoked parcellation reconfigurations are robust and reliable not only across different sessions, but also across distinct individuals.

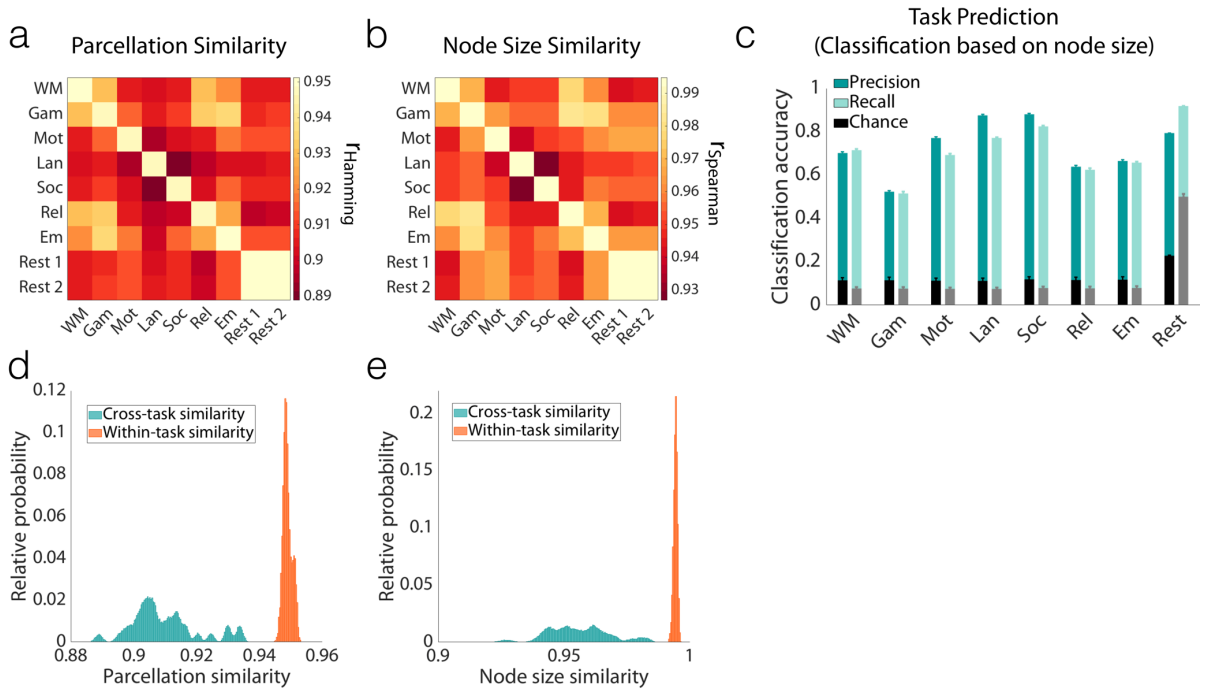

Figure 4. Replication of the finding that node definitions change with task condition, even when considered across individuals; Human Connectome Project (HCP) data. a) Pairwise parcellation similarity was calculated within and across functional conditions (9 conditions, N=514 subjects), using voting-based ensemble analysis with 1000 iterations. The matrix represents the average over all iterations. Similarity was assessed by $r_{Hamming}$ =1-Hamming distance. b) The same analysis as (a) was performed, this time using rank correlation of node-size vectors ($r_{Spearman}$) as a proxy for parcellation similarities. c) The bars report the accuracy of predicting the functional condition using 10-fold cross-validated GBM classifier with node sizes as features, iterated 100 times. The predictive power is measured by precision (dark cyan) and recall (light cyan) values for each condition (reported as mean ± s.d. across iterations). The precision (black) and recall (gray) values of the 1000 null models are also reported (error bars represent ±s.d.). d) A histogram of the parcellation similarities for all 1000 iterations is depicted for within-condition (diagonal elements in [a]) and cross-condition (off-diagonal elements in [a]) comparisons. The two distributions are significantly different (KS-test; $p<0.001$). e) A histogram of the node size similarities for all 1000 iterations is depicted for within-condition (diagonal elements in [b]) and cross-condition (off-diagonal elements in [b]) comparisons. The two distributions are significantly different (KS-test; $p<0.001$).

Robustness of the state-evoked atlas reconfiguration across scales

In our final analysis, we sought to address the question of parcellation scale, asking if these reconfigurations are simply due to the rather large node sizes typically targeted in current parcellation approaches. In the limit of nodes reduced to the size of a voxel, there can be no condition-induced change in node definition since the node is defined by the voxel size. Here we attempted to determine the critical resolution at which parcellations stabilize. To address

this question, we repeated our analyses with Yale data, using atlases containing greater numbers of nodes, from 368, to 1041, to 5102 nodes. In each case, similar results were obtained, even when the number of nodes was increased to 5102, more than ten times the typical number of nodes used in functional connectivity analysis (Figure 5a-d)[34-36]. See Figure S2 and S3 for the results with 368-node and 1041-node atlases, respectively. To date, the parcellation community has not considered atlases in the 5000 node and higher range.

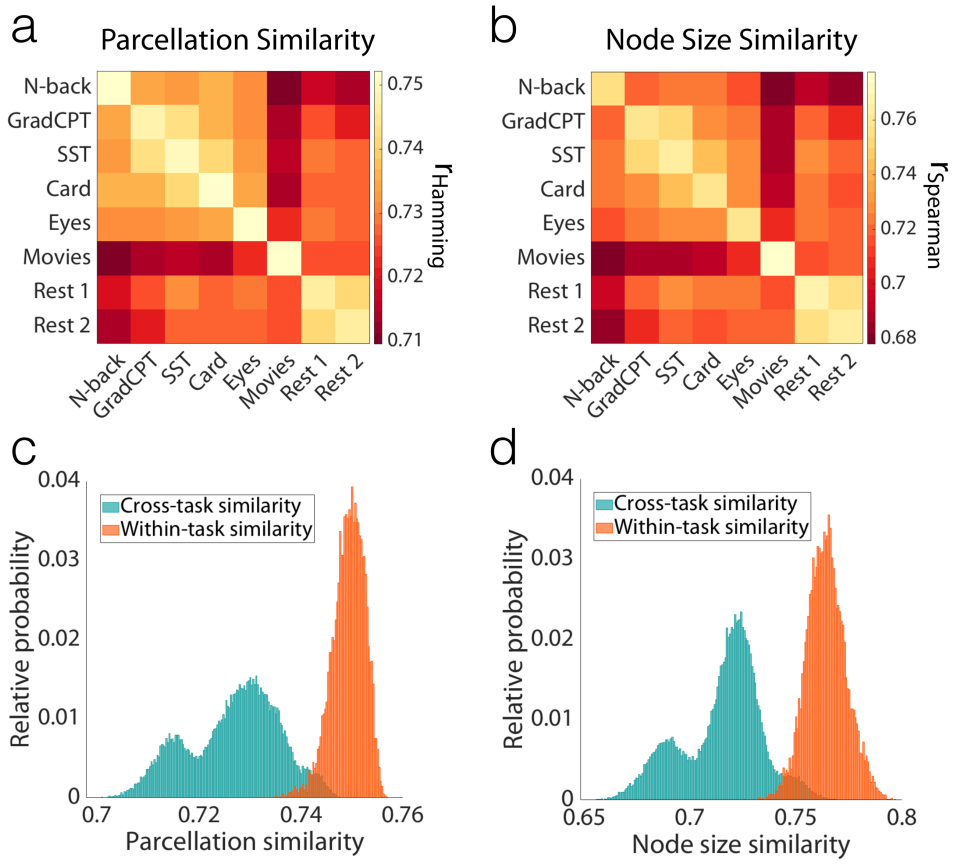

Figure 5. Node size effects: Even for an atlas with 5102 nodes (on average 25 voxels per node), node definitions change with task condition, with high reliability within conditions. a) Pairwise parcellation similarity was calculated within and across functional conditions, using voting-based ensemble analysis with 1000 iterations. Similarity was assessed by $r_{Hamming}$ =1-Hamming distance. b) The same analysis as (a) was performed, this time using rank correlation of node-size vectors ($r_{Spearman}$) as a proxy for parcellation similarities. c) The histogram of the parcellation similarities for all 1000 iterations is depicted for within-condition (diagonal elements in [a]) and cross-condition (off-diagonal elements in [a]) comparisons. The two distributions are significantly different (KS-test; $p<0.001$). d) The histogram of the node size similarities for all 1000 iterations is depicted for within-condition (diagonal elements in [b]) and cross-condition (off-diagonal elements in [b]) comparisons. The two distributions are significantly different (KS-test; $p<0.001$).

Discussion

Together, these findings suggest that there is no single functional atlas for the human brain. The parcellation boundaries of functionally defined nodes change with changes in brain state in a consistent and reproducible manner. These node reconfigurations appear to be cognitively and biologically meaningful, as evidenced by their utility in predictive models of task condition and within-condition task performance.

Reconfiguration of the connectome

These results are consistent with the extensive evidence for reconfigurations of the connectome. There is growing evidence that patterns of functional connectivity change with changing brain states (e.g., as induced by distinct tasks), and that these changes are functionally significant[37]. Recent work has highlighted the impact of node spatial configuration across individuals on brain-behavior relationships[30], but the common assumption that node boundaries are fixed for a given individual remains unchallenged; in fact, as we demonstrate, task-induced node reconfigurations are substantial, consistent, and functionally significant both within and across individuals, and taking such reconfigurations into account may further inform efforts to relate changing patterns of functional connectivity to behavior and cognition.

The generalizability of the state-evoked node reconfigurations across a large cohort of individuals, as demonstrated by the HCP data (Figure 4), is important. Previous work has shown that patterns of functional connectivity are unique to each individual[38], and any state-evoked reconfigurations are also individual-specific[39]. That the average of these state-evoked node reconfigurations across individuals does not mask out the effect of state is a significant finding, suggesting that task-induced node reconfigurations are not idiosyncratic and subject-specific, but rather robust and generalizable; that is, despite significant individual differences in brain functional organization, task-induced brain states have consistent and substantial effects on this organization.

Composition of functional subunits

The cause of such node reconfigurations remains an important open question. At the atlas sizes considered here, any individual node will contain hundreds of thousands of neurons. Node boundaries may change as different subsets of neurons within a given node are engaged to subserve a particular function. If this is the case then it is possible that consistent invariant boundaries may not be found until the acquisition resolution is of the order of cortical columns (300-500 μm)[40,41] or less. The findings here, of substantial node reconfiguration occurring even at atlas sizes of 5000 nodes (consisting of, on average, 25, 2mm^3 voxels, or ~5.8 mm^3 of tissue), suggest that the minimal functional units that we wish to identify are much smaller than ~5.8 mm, and not of the order of 200-400 node atlases, which have previously been suggested to delineate minimal functional units [7,35,36]. Nevertheless, our goal does not have to be to identify a minimal functional unit. In practice a unit that has a homogeneous, distinct identity in a given state is sufficient for many analyses. In other

words, as long as the atlas is consistent with the state of interest, atlases in the 400-node range are entirely appropriate, and we may not need to know the size of the minimal functional unit.

Additional considerations

The exemplar-based clustering approach used in this work imposes a constraint that holds the total number of nodes fixed. In doing so, it eliminates the problem of establishing correspondence between nodes under different conditions. Maintaining node correspondence across parcellations allows for quantitative assessment of the change in each node. It is possible that nodes not only reconfigure, but also blend and/or split, leading to a change in the total number of nodes with a change in brain state or function. This additional degree of freedom would make comparison of atlases across conditions more difficult due to the correspondence problem but nevertheless the conclusion would be the same: there is no fixed functional atlas at the scale typically used in functional MRI studies.

States are defined in this work as task conditions with acquisitions spanning a series of continuous performance, event-related, and blocked tasks. It is likely that node reconfiguration occurs over considerably shorter periods of time than these ~6-minute task intervals. Future work may seek to characterize how node boundaries continuously vary to reflect the dynamic reconfiguration of macroscale neural circuitry underlying moment-to-moment changes in brain state.

This work also does not invalidate multimodal parcellation approaches that combine both anatomical and functional data (including functional data across a wide range of task- and resting-states) but suggests, instead, that those approaches are defining a mean atlas across states, thereby masking important information on specific node reconfigurations associated with specific brain states.

Implications

Essentially all publications to date have used fixed atlases. Such fixed nodes may be defined anatomically or functionally (or through a combination of methods) but nevertheless, the underlying assumption of a fixed functional subunit is not correct. The findings here, for the most part, do not invalidate these previous works. But they do potentially impact the interpretation of the changes in connectivity observed. The findings here suggest that changes in connectivity could be attributable in part to reconfiguration of the nodes.

It has been posited that imposing an atlas on the brain is simply a data-reduction strategy to reduce the connectivity matrix to a manageable size. This may indeed be a useful feature (for a discussion see Eickhoff et al.[19]), and this work does not impact the utility of that approach. The findings here, however, support the notion that function-based parcellations are not only a means of data dimensionality reduction but also a way to identify meaningful functional subunits. The results demonstrating prediction of state and performance based on the particular node configuration support this conclusion.

This work has immediate implications for investigators developing algorithms aimed at finding the ideal parcellation, by refocusing the goal to understanding state-specific organization at the nodal level. New approaches to individualized parcellation, such as the approach used in this work, could potentially lead to custom state-dependent atlases for individuals or groups. Much work needs to be done to understand the relationship between functional edge strength measures and these variable node configurations, and the impact of these variables on graph theory measures in both healthy populations and disease. It is an open question as to whether fixed minimal functional subunits, invariant to task or brain state, can be defined in the human cortex with current state-of-the-art neuroimaging methods.

Conclusion

This work demonstrates that there is no single functional atlas for the human brain at the 200-5000 node resolution level, but rather that nodes reconfigure depending on task in a robust and reliable manner. Such reconfigurations are distinct and reliable enough to allow prediction of the task condition across multiple tasks as well as within-task performance, directly from quantitative node characteristics (i.e., node size). That functional node definitions are fluid must be considered when interpreting changes in connectivity in graph theory or other connectivity analyses across brain states. The results highlight the importance of considering state-evoked variations in node definitions and leveraging state-specific individualized functional atlases for functional connectivity analyses, and call for the continued development and validation of such approaches.

Materials and Methods

Three data sets were used in this work. The primary data were collected at Yale University from one healthy subject (author R.T.C.). The validation data were obtained from the publicly available Midnight Scan Club (MSC) dataset[31], and Human Connectome Project (HCP). These three data sets are described in detail below.

Yale Data

Participant and Processing

The primary subject R.T.C. is a healthy left-handed male, aged 56 years old at the onset of the study.

R.T.C. was scanned at Yale University 33 times (that is, 33 sessions) over ten months. Scans were typically performed on Wednesdays at 8:30 am and Fridays at 2:00 pm. Functional MRI data were acquired on 2 identically configured Siemens 3T Prisma scanners equipped with a 64-channel head coil at Yale Magnetic Resonance Research Center. Three sessions were excluded from analysis: the first two sessions were excluded because of the considerable adjustment in task design after session 2, and the ninth session was excluded due to interruptions in task presentation due to computer software changes.

The first session was used to acquire structural MRI data. High-resolution T1-weighted 3D anatomical scans were performed using a magnetization prepared rapid gradient echo (MPRAGE) sequence with the following parameters: 208 contiguous slices acquired in the sagittal plane, repletion time (TR) = 2400 ms, echo time (TE) = 1.22 ms, flip angle = 8°, slice thickness = 1 mm, in-plane resolution = 1 mm × 1 mm, matrix size = 256 × 256. A T1-weighted 3D anatomical scan was acquired using a fast low angle shot (FLASH) sequence with the following parameters: 75 contiguous slices acquired in the axial-oblique plane parallel to AC-PC line, TR = 440 ms, TE = 2.61 ms, flip angle = 70°, slice thickness = 2 mm, in-plane resolution = 0.9 mm × 0.9 mm, matrix size = 256 × 256.

Functional scans were performed using a multiband gradient echo-planar imaging (EPI) pulse sequence with the following parameters: 75 contiguous slices acquired in the axial-oblique plane parallel to AC-PC line, TR = 1000 ms, TE = 30 ms, flip angle = 55°, slice thickness = 2 mm, multiband = 5, acceleration factor = 2, in-plane resolution = 2 mm × 2 mm, matrix size = 110 × 110.

Data were analyzed using BioImage Suite[42] and custom scripts in MATLAB (MathWorks). Motion correction was performed using SPM12 (http://www.fil.ion.ucl.ac.uk/spm/software/spm12/). White matter and CSF masks were defined in MNI space and warped to the single-subject space using a series of linear and non-linear transformations (see Scheinost et al.[43]). The following noise covariates were regressed from the data: linear, quadratic, and cubic drift, a 24-parameter model of motion[44], mean cerebrospinal fluid signal, mean white matter signal, and mean global signal. Finally, data

were temporally smoothed with a zero mean unit variance Gaussian filter (cutoff frequency=0.19 Hz).

Dimensional Task Battery Design

Functional scans were 6 minutes 49 seconds each, including initial shim and 8s discarded acquisitions before the start of each task. Tasks varied slightly in length (see below), but were all approximately 6 minutes in duration. A fixation cross was displayed after the end of each task and lasted until the beginning of the next task. Each task, with the exception of movie watching, was preceded by instructions and practice, after which the subject had the opportunity to ask questions before the scan began. All responses were recorded using a 2×2 button box.

Each session consisted of two resting-state runs and six task runs. The first and last functional runs (runs 1 and 8) were resting-state runs, during which the participant was instructed to stay still with his eyes open. Runs 2-7 were task runs, with the order counterbalanced via Latin Square across sessions.

Task Details

N-Back Task

The *n*-back task was adapted from that used in Rosenberg et al.[23]. In this task, the participant was presented with a sequence of images and was instructed to respond via button press if the image was different than the image presented two before, and to withhold response if it was the same. Images were presented for 1 second, followed by a 1-second inter-trial interval (ITI; fixation cross). The target (i.e., matching image) probability was 10%. There were two blocks, each with 90 trials. One block used images of emotional faces and the other block used images of scenes[45,46]. Block and stimulus order were randomized for each session. Task performance was assessed by *sensitivity* (*d'*), defined as hit rate relative to false alarm rate[25].

Gradual-onset Continuous Performance Task (gradCPT)

The gradCPT task was adapted from that described in Esterman et al.[24] and Rosenberg et al.[25,26]. In this task, the participant viewed a sequence of 450 scenes [city or mountain] that gradually transitioned via linear pixel-by-pixel interpolation from one to the next over 800ms. The participant was instructed to respond via button press to cities and to withhold response to mountains. Stimulus order was randomized, and 10% of images were mountains. Task performance was assessed by *sensitivity* (*d'*).

Stop-Signal Task (SST)

The stop-signal task was adapted from that implemented in Verbruggen et al.[27]. In this task, the participant was required to determine via button press whether a presented arrow was pointing left (right index finger) or right (right middle finger). On 25% of trials, the arrow turned blue after some delay, indicating that the participant should withhold response. This stop-signal delay (SSD) was initially set to 250ms, and was continuously adjusted via the

staircase tracking procedure (50ms increase after correct inhibition trials; 50ms decrease after each failure to inhibit). The arrow was presented for 1.5 seconds, followed by 0.5 seconds of fixation; there were 176 trials in total, with stimulus order randomized within block. Task performance was assessed by *missing probability*, defined as the percentage of missed responses on no-signal trials[27].

Card Guessing Task

The card guessing task was adapted from that originally developed by Delgado et al.[28] and subsequently extended[47,48]. In this task, the participant was presented with a card and asked to guess if the number on the back was lower than 5, or greater than 5 but less than 10. The question mark card was displayed for 1.5 seconds, or until the participant responded (right index finger for "lower," right middle finger for "higher"). The card then "flipped over" to reveal the number. The number was displayed for 0.5 seconds, followed by an arrow for 0.5 seconds to indicate accuracy (green and up for correct, red and down for incorrect), which was in turn followed by a 1-second inter-trial interval (fixation cross). There were 10 blocks, each with 10 trials, and guess accuracy was deterministic, such that in half of the blocks ("high win"), the participant was correct 70% of the time, while in the other half of the blocks ("high loss") he was correct 30% of the time; block (high win/loss) and trial (correct/incorrect) orders were randomized. Task performance was assessed by *RT variability*, defined as standard deviation of reaction time for correct trials[49].

Reading the Mind in the Eyes Task ("Eyes Task")

The Eyes Task was adapted from that originally described in Baron-Cohen et al.[29]. In this task, the participant viewed a series of photographs of an individual's eyes with four "mental state terms"[29], one in each corner of the image, and was instructed to select via button press (with each button corresponding to one corner, and thus one term) the term that best described what the individual was thinking or feeling. There were 36 images in total. Each was presented once, in random order, for 9.25 seconds or until the participant responded; the remainder of each 10-second trial consisted of a fixation cross. Task performance was assessed by *RT variability*.

Movies Task

In this task, three movie clips were presented in continuous series; each was approximately 2 minutes long. The first clip was a trailer for "Inside Out," the second clip was the wedding scene from "Princess Bride," and the third clip was a trailer for "Up;" order was fixed across sessions. The participant was instructed to relax and enjoy the movies; no responses were required. No task performance was recorded.

Midnight Scan Club (MSC) Data

Participants and Processing

The MSC data set[31] includes data from 10 healthy individuals (5 females; age=24-34); each underwent 1.5s hour of functional MRI scanning on 10 consecutive days, beginning at midnight. For details of the data acquisition parameters and sample demographics see Gordon et al[31]. Two individuals were excluded from the analysis: MSC08 was excluded because of excessive head motion and self-reported sleep[31]; MSC10 was excluded for insufficient data (missing one session of incidental memory task).

All data were preprocessed using BioImage Suite[42]. Data were transformed to MNI space to facilitate analysis across multiple subjects. Preprocessing steps included regressing 24 motion parameters, regressing the mean time courses of the white matter and cerebrospinal fluid as well as the global signal, removing the linear trend, and low pass filtering.

Task Battery Design

Each scanning session started with a 30-min resting-state fMRI scan, followed by three separate task-based fMRI scans: motor (2 runs per session, 7.8 min combined), incidental memory (3 runs per session, 13.1 min combined), and semantic-coherence design (2 runs per session, 14.2 min combined).

Motor Task

The motor task was adapted from that used in the Human Connectome Project (HCP)[47]. In this task, participants were cued to perform one of the following movements: closing/relaxing their hands, flexing/relaxing their toes, or wiggling their tongue. Each block started with a 2.2 s cue indicating which movement to perform, followed by a central caret (flickering every 1.1s) to signal the movement. Each run consisted of 2 blocks of each movement type and 3 blocks of resting-fixation (15.4 s total).

Incidental Memory Task

The incidental memory task consisted of three different types of stimuli (scenes, faces, and words), each presented in a separate run. For scene runs, participants were asked to decide if the presented scene was indoors or outdoors. For face runs, participant made male/female judgments. For word runs, participants made abstract/concrete judgments. Each run consisted of 24 stimuli, each repeating 3 times. Stimuli were presented for 1.7 s with a jittered 0.5-4.9 s inter-stimulus interval. All stimuli were taken from publicly available sources (see Gordon et al.[31] for details).

Semantic-Coherence Task

The semantic-coherence task had a mixed block/event-related design, consisting of two different conditions ("semantic" and "coherence"). In the "coherence" task, participants viewed a concentric dot pattern (Glass[50]) with 0% or 50% coherence, and made binary decisions whether the pattern was concentric or random. In the semantic task, participants viewed a word and indicated whether the word is a noun or verb. Each run consisted of two blocks of each task, separated by 44 s of rest. Each block started with a 2.2 s cue indicating which task was to be performed. Blocks consisted of 30 trials. Stimuli were presented for 0.5

s with a variable 1.7-8.3 s ISI. Each block finished with a 2.2 s cue indicating the end of the task block.

Human Connectome Project (HCP) Data

Participants and Processing

The HCP data set[33] includes data from 897 healthy individuals (S900) scanned during nine functional conditions (seven tasks and two rest). For details of the data acquisition parameters see Uğurbil et al.[51] and Smith et al[52]. Analyses were restricted to subjects for whom data were available for all nine functional conditions (with left-right (LR) and right-left (RL) phase encoding). To mitigate the substantial effects of head motion on functional parcellations, we further excluded subjects with excessive head motion (defined as mean frame-to-frame displacement > 0.1 mm and maximum frame-to-frame displacement > 0.15 mm), leaving 514 subjects (284 females; age = 22-36+) for analysis.

The HCP minimal preprocessing pipeline was employed[53], which includes artifact removal, motion correction and registration to MNI space. Further preprocessing steps were performed using BioImage Suite[42] and included standard preprocessing procedures[38] including regressing 24 motion parameters, regressing the mean time courses of the white matter and cerebrospinal fluid as well as the global signal, removing the linear trend, and low pass filtering.

Task Battery Design

Functional MRI scans were acquired during two different days: Day 1 included two runs (LR and RL) of the working memory (WM) task (5:01 min per run), incentive processing (gambling) task (3:12 min), motor task (3:34 min), and rest (14:33 min); day 2 included two runs of the language processing task (3:57 min), social cognition (theory of mind) task (3:27 min), relational processing task (2:56 min), emotion processing task (2:16 min), and rest (14:33 min).

The details of task design have been previously described[33,47]. We provide a brief description of each task and an overview of the relevant aspects below.

Working Memory Task

In this task, participants performed a visual *n*-back task, with blocked 0-back and 2-back conditions using four stimulus categories (faces, places, tools, body parts). Each run consisted of 8 task blocks (10 trials each), with each stimulus category used twice, and 4 fixation blocks. Each block started with a 2.5 s cue indicating the task type (0-back versus 2-back) and the target (for 0-back).

Gambling Task

In this task, participants were presented with a mystery card and asked to guess if the number on the back was lower than 5, or greater than 5 but less than 10. On reward trials, participants

were shown the number on the card, a green up arrow, and "$1"; on loss trials, participants were shown the number on the card, a red down arrow, and "-$0.50"; on neutral trials, participants were shown the number 5 and a gray, double-headed arrow. Each run consisted of 4 task blocks (8 trials each) and 4 fixation blocks. In half of the blocks ("mostly reward"), subjects were correct in 6 out of 8 trials (the remaining 2 trials were either neutral or loss), while in the other half of the blocks ("mostly loss") they were incorrect in 6 out of 8 trials (the remaining 2 trials were either neutral or reward).

Motor Task

Participants were presented with visual cues that asked them to tap their left or right fingers, squeeze their left or right toes, or move their tongue. Each block started with a 3 s cue indicating which movement to perform. Each run consisted of 2 blocks of tongue movements, 4 blocks of hand movements (2 left and 2 right), 4 blocks of foot movements (2 left and 2 right), and 3 blocks of resting-fixation.

Language Task

In this task, participants were aurally presented with 4 blocks of a story task and 4 blocks of a math task. In the story task, they heard brief fables (5-9 sentences) and completed two-alternative forced-choice questions about the topic of the story. In the math task, they completed addition and subtraction problems in a two-alternative forced-choice setting.

Social Task

In this task, participants were presented with 20-s video clips of objects (squares, circles, triangles) either interacting (theory-of-mind) or moving randomly. Participants were asked to choose between three potential responses ("mental interaction", "no mental interaction", and "not sure"). Each run consisted of 5 video blocks (2 mental and 3 random in one run, 3 mental and 2 random in the other run) and 5 fixation blocks.

Relational Task

The relational task consisted of two different conditions ("relational" and "matching"). In the relational condition, participants were presented with two pairs of objects with one pair at the top and the other pair at the bottom of the screen. They were asked to decide whether the bottom pair of objects differed along the same dimension (i.e., shape or texture) as the top pair. In the control matching condition, they were presented with two objects at the top, one object at the bottom, and a word ("shape" or "texture") in the middle of the screen. They were asked to determine whether the bottom object matched either of the top two objects on the dimension specified by the word. Each run consisted of 3 relational blocks (4 trials each), 3 matching blocks (5 trials each) and 3 fixation blocks.

Emotion Task

In this task participants were presented with blocks of "face" and "shape" tasks, and were asked to determine which of the two faces (or shapes) presented at the bottom of the screen matched the face (or shape) at the top of the screen. Faces had either angry or fearful

expressions. Each block started with a 3 s cue indicating which task to perform. Each run included 3 face blocks (6 trials each) and 3 shape blocks (6 trials each), with 8 s fixation at the end of each run.

Node-level Parcellation Algorithm: Individual- and State-specific Approach

Here, we extended our previously developed individualized parcellation algorithm (Salehi et al.[10]) to account for the spatial contiguity of the nodes at the individual level. The presented algorithm is a priority-based submodular method that defines functional nodes in a streaming fashion, for every individual in every functional state.

Our algorithm runs in three steps:

i. **Registration of the initial group-level parcellation.** In the first step, an off-the-shelf group-level parcellation is applied to each individual's data, assigning each voxel to a node defined by the group parcellation. At this step, all individuals in every state have the same node definitions.
ii. **Exemplar identification.** In the second step, for every group-defined node in an individual brain, an exemplar is identified by maximizing a monotone nonnegative submodular function (see Eq. 2).
iii. **Spatially-constrained voxel-to-node assignment.** Finally, the third step assigns every voxel in each individual brain to the functionally closest exemplar, ensuring the spatial contiguity of the resulting node.

Exemplar Identification

The exemplar identification algorithm can be viewed as a data summarization step, where the goal is to summarize a massive amount of data by fewer representative points or exemplars. A classic way of defining such exemplars is by finding the set S that minimizes the following loss function, subject to the constraint $|S| = k$ (known as k-medoid problem).

$$L(S) = \frac{1}{|V|}\sum_{v\in V} \min_{e\in S} d(v,e). \quad (1)$$

In this equation, V is the ground set consisting of all data points, $d: V \times V \to R$ is a dissimilarity function defined on every pair of data points, and S is the objective exemplar set. Intuitively, $L(S)$ measures how much information we lose if we summarize the entire ground set to the exemplar set by representing each data point with its closest exemplar.

Minimizing this loss function (1) is NP-hard, as it requires exponentially many inquiries. Using an appropriate auxiliary exemplar v_0, we transform the minimization of (1) into the maximization of a non-negative monotone submodular function[54], for which general greedy algorithms provide an efficient $1 - 1/e \approx 0.63$ approximation to the optimal solution:

$$\max_{S \subseteq V} f(S) \quad s.t.\ |S| \leq k, \tag{2}$$

where:

$$f(S) = L(v_0) - L(S \cup v_0). \tag{3}$$

In practice, the greedy algorithm provides a considerably closer approximation to the optimal solution (see Salehi et al.[55]). For the choice of auxiliary exemplar, any vector v_0 whose distance to every data point is greater than the pair-wise distances between data points can be used.

Definition 1.2 (Submodularity) A function $f: 2^V \rightarrow R$ is submodular if for every $A \subseteq B \subseteq V$ and $e \in V \backslash B$ it holds that $f(A \cup e) - f(A) \geq f(B \cup e) - f(B)$. That is, adding an element e to a set A increases the utility at more than (or at least equal to) adding it to A's superset, B, suggesting a natural diminishing returns.

Spatially-Constrained Voxel-to-Node Assignment

After identification of all exemplars (one per node), every voxel in the individual brain is assigned to the functionally closest exemplar while taking the spatial contiguity of the node into account. The spatial contiguity is assured by utilizing priority queues. Every exemplar i is assigned a priority queue (denoted as q_i). Initially, all the queues are empty. In the first round, spatial neighbors of exemplar i are pushed into q_i. The voxels in each queue are sorted according to their functional distance to the corresponding exemplar such that the voxel with minimum functional distance (maximum similarity) is in front. Next, the front voxel in each q_i is considered as a potential candidate for being assigned the label i. Among all these candidates, the one with minimum distance to its corresponding exemplar is selected and assigned the exemplar's label. Next, this voxel is popped out of the queue, and all of its spatial neighbors are pushed into the same queue. The algorithm continues until all the voxels are assigned a label. Note that at every step of the algorithm the labeled voxel is ensured to be spatially connected to its exemplar (either directly or through other previously labeled voxels).

Implementation Details

Here, we implemented an accelerated version of the greedy algorithm, called lazy greedy[56]. Also, here $k = 1$, as we attempt to identify one exemplar per node (see Salehi et al.[10] for details of interpretation and alternative approaches). For the choice of dissimilarity measure, we used squared Euclidean distance, after normalizing all the voxel-level time courses to a unit norm sphere centered at the origin. A point with the norm greater than two was used as the auxiliary exemplar. The parcellation algorithm was applied to each fMRI run (each individual in each state) independently, and thus was efficiently employed through parallelization. For HCP data, we restricted our analysis to left-right (LR) phase encoding.

Initial Group-Level Parcellations

As the initial group-level parcellation, we primarily used a 268-node atlas, previously defined in our lab using a spectral clustering algorithm on resting-state data of a healthy population[14,38]. We replicated the results with more fine-grained atlases including 368, 1041, and 5102 nodes. The 368-node atlas was defined by integrating the parcellation of cortex from Shen et al.[14], subcortex from the anatomical Yale Brodmann Atlas[57], and cerebellum from Yeo et al.[58]. Similarly, the 1041-node parcellation was defined by integrating the subcortical and cerebellum portion of the 368-node parcellation with the 1000-node cortex parcellation from Yeo et al[58]. To define the 5102-node atlas, we started from the 1041-node parcellation and randomly divided all the nodes until the number of voxels per node reached approximately 25.

Statistical Ensemble Analysis

To estimate the similarity of parcellations within and across states, we employed an ensemble analysis. For each condition, we divided all sessions (for Yale and MSC data) or individuals (for HCP data) into two equal-size groups: group 1 and group 2. We took the majority vote over the parcellations of each group, resulting in two parcellations for each functional state, one for each group. Next, we assessed the similarity between every pair of the non-overlapping parcellations both within and across states. For instance, if there are m functional states, this analysis generates an $m \times m$ matrix, where each element (i, j) represents the similarity between the parcellation of group 1 for state i and the parcellation of group 2 for state j. Thus, the diagonal elements represent the within-state similarities while the off-diagonal elements represent the cross-state similarities. We repeated the entire analysis 1000 times, generating an ensemble of $m \times m$ similarity matrices. The normalized distribution of the within-state and cross-state similarity values were depicted as histograms, and compared using non-parametric Kolmogorov–Smirnov test (Figure 2d,e, 3d,e, and 4d,e). The average of these similarity matrices were also displayed (Figure 2a,b, 3a,b, and 4a,b).

Similarity Measures Between Parcellations

We compared parcellations at two different scales: at the fine-scale, we studied the ratio of voxels that change their node assignment across different parcellations. The fine-scale similarity was calculated using 1-Hamming distance (Figure 2a, 3a, 4a). At the coarse scale, we studied the changes in the node sizes across parcellations. The coarse-scale similarity was computed using Spearman correlation between node-size vectors (Figure 2b, 3b, 4b).

Functional State Decoding Using Node Size as Feature

We established a fully cross-validated predictive model that predicts the functional state of each unseen sample solely based on the size of nodes in that parcellation. Using a k-fold cross-validated approach, we trained and tested a gradient boosting classifier (GBM; with 300 estimators and learning rate = 0.1) using node sizes as features and the functional state as output. We randomly divided the entire data into k folds (k=n for the Yale and MSC data sets and k=10 for the HCP data set). At each step, the model was trained on k-1 folds and tested to predict the state of the left-out fold. The predictive power of the model was estimated using

precision (also known as positive predictive value) and recall (also known as sensitivity), calculated separately for each state. Both precision and recall measures range between 0 and 1, with higher values indicating higher predictive power. Precision calculates what fraction of the retrieved instances were actually relevant, while recall expresses what fraction of relevant instances were retrieved. In the case of 10-fold cross-validation (i.e., for the HCP data set), we repeated the predictive analysis 100 times to account for the randomness of the folds, and reported the precision and recall measures as the mean and standard deviation across all iterations.

To evaluate the significance of the results, we employed non-parametric permutation testing: we randomly permuted the output vector (here the functional states) 1000 times, and each time ran the permuted values through the same predictive pipeline and calculated the precision and recall measures of the permuted states.

Task Performance Prediction Using Node Size as Feature

To establish the relevance of parcellation boundary changes to within-task variation in brain state, we developed a fully cross-validated predictive pipeline that predicts task performance during each session from the node sizes in the parcellation of that session. Using a leave-one-out cross-validated approach, we trained and tested a ridge regression model (with regularization parameter = 1), using node sizes as features and the performance scores as output. For each task, a model was trained on n-1 sessions (of that task) and used to predict performance for the left-out session. Analyses were performed for each task independently. To measure performance, we used *d'* for *n*-back and gradCPT tasks, *RT variability* for eyes and card-guessing tasks, and *missing probability* for SST task. The predictive power was estimated using r-values, defined as the square root of the percentage of the explained variance. To estimate the significance of the results, we employed non-parametric permutation testing, where we randomly permuted the behavioral scores 1000 times, and each time ran the permuted scores through the predictive pipeline and calculated the R-value. P-values were also calculated from the permutation test (instead of the traditional r-to-p conversions).

Code and Data Availability

All the functional parcellations are available online on the BioImage Suite NITRC page (https://www.nitrc.org/frs/?group_id=51). MATLAB, C++ (for parcellation algorithm), and Python (for predictive modeling) scripts were written to perform the analyses described; these codes are available on GitHub at https://github.com/YaleMRRC/Node-Parcellation.git. The force-directed graph visualization (R script) is released separately under the terms of GNU General Public License and can be found here: https://github.com/YaleMRRC/Network-Visualization.git. The data that support the findings of this study are publicly available in International Neuroimaging Data-sharing Initiative (INDI) [http://fcon_1000.projects.nitrc.org/].

References

1 Brodmann, K. *Vergleichende Lokalisationslehre der Grosshirnrinde in ihren Prinzipien dargestellt auf Grund des Zellenbaues*. (Barth, 1909).

2 Tzourio-Mazoyer, N. *et al.* Automated anatomical labeling of activations in SPM using a macroscopic anatomical parcellation of the MNI MRI single-subject brain. *Neuroimage* **15**, 273-289 (2002).

3 McIntosh, A. *et al.* Network analysis of cortical visual pathways mapped with PET. *Journal of Neuroscience* **14**, 655-666 (1994).

4 Downing, P. E., Jiang, Y., Shuman, M. & Kanwisher, N. A cortical area selective for visual processing of the human body. *Science* **293**, 2470-2473 (2001).

5 Schubotz, R. I., Anwander, A., Knösche, T. R., von Cramon, D. Y. & Tittgemeyer, M. Anatomical and functional parcellation of the human lateral premotor cortex. *Neuroimage* **50**, 396-408 (2010).

6 Craddock, R. C., James, G. A., Holtzheimer, P. E., Hu, X. P. & Mayberg, H. S. A whole brain fMRI atlas generated via spatially constrained spectral clustering. *Human brain mapping* **33**, 1914-1928 (2012).

7 Nieuwenhuys, R., Broere, C. A. & Cerliani, L. Erratum to: A new myeloarchitectonic map of the human neocortex based on data from the Vogt-Vogt school. *Brain structure & function* **220**, 3753-3755, doi:10.1007/s00429-014-0884-8 (2015).

8 Chong, M. *et al.* Individual parcellation of resting fMRI with a group functional connectivity prior. *NeuroImage* **156**, 87-100 (2017).

9 Blumensath, T. *et al.* Spatially constrained hierarchical parcellation of the brain with resting-state fMRI. *Neuroimage* **76**, 313-324 (2013).

10 Salehi, M., Karbasi, A., Scheinost, D. & Constable, R. T. in *International Conference on Medical Image Computing and Computer-Assisted Intervention.* 478-485 (Springer).

11 Smith, S. M. *et al.* Functional connectomics from resting-state fMRI. *Trends in cognitive sciences* **17**, 666-682, doi:10.1016/j.tics.2013.09.016 (2013).

12 Gordon, E. M. *et al.* Generation and evaluation of a cortical area parcellation from resting-state correlations. *Cerebral cortex* **26**, 288-303 (2014).

13 Power, J. D. *et al.* Functional network organization of the human brain. *Neuron* **72**, 665-678, doi:10.1016/j.neuron.2011.09.006 (2011).

14 Shen, X., Tokoglu, F., Papademetris, X. & Constable, R. T. Groupwise whole-brain parcellation from resting-state fMRI data for network node identification. *Neuroimage* **82**, 403-415 (2013).

15 Thomas Yeo, B. T. *et al.* The organization of the human cerebral cortex estimated by intrinsic functional connectivity. *Journal of Neurophysiology* **106**, 1125-1165, doi:10.1152/jn.00338.2011 (2011).

16 Fan, L. *et al.* The human brainnetome atlas: a new brain atlas based on connectional architecture. *Cerebral cortex* **26**, 3508-3526 (2016).

17 Glasser, M. F. *et al.* A multi-modal parcellation of human cerebral cortex. *Nature* **536**, 171-178 (2016).

18 Van Essen, D. C. Cartography and connectomes. *Neuron* **80**, 775-790, doi:10.1016/j.neuron.2013.10.027 (2013).

19 Eickhoff, S. B., Constable, R. T. & Yeo, B. T. Topographic organization of the cerebral cortex and brain cartography. *Neuroimage* **170**, 332-347 (2018).

20 Fox, P. T. & Lancaster, J. L. Mapping context and content: the BrainMap model. *Nature Reviews Neuroscience* **3**, 319 (2002).

21 Yarkoni, T., Poldrack, R. A., Nichols, T. E., Van Essen, D. C. & Wager, T. D. Large-scale automated synthesis of human functional neuroimaging data. *Nature methods* **8**, 665 (2011).

22 Eickhoff, S. B. *et al.* Co-activation patterns distinguish cortical modules, their connectivity and functional differentiation. *Neuroimage* **57**, 938-949 (2011).

23 Rosenberg, M. D., Finn, E. S., Constable, R. T. & Chun, M. M. Predicting moment-to-moment attentional state. *Neuroimage* **114**, 249-256 (2015).

24 Esterman, M., Noonan, S. K., Rosenberg, M. & DeGutis, J. In the zone or zoning out? Tracking behavioral and neural fluctuations during sustained attention. *Cerebral Cortex*, bhs261 (2012).

25 Rosenberg, M. D. *et al.* A neuromarker of sustained attention from whole-brain functional connectivity. *Nat Neurosci* **19**, 165-171, doi:10.1038/nn.4179 http://www.nature.com/neuro/journal/v19/n1/abs/nn.4179.html#supplementary-information (2016).

26 Rosenberg, M., Noonan, S., DeGutis, J. & Esterman, M. Sustaining visual attention in the face of distraction: a novel gradual-onset continuous performance task. *Attention, Perception, & Psychophysics* **75**, 426-439 (2013).

27 Verbruggen, F., Logan, G. D. & Stevens, M. A. STOP-IT: Windows executable software for the stop-signal paradigm. *Behavior research methods* **40**, 479-483 (2008).

28 Delgado, M. R., Nystrom, L. E., Fissell, C., Noll, D. & Fiez, J. A. Tracking the hemodynamic responses to reward and punishment in the striatum. *Journal of neurophysiology* **84**, 3072-3077 (2000).

29 Baron-Cohen, S., Jolliffe, T., Mortimore, C. & Robertson, M. Another advanced test of theory of mind: Evidence from very high functioning adults with autism or Asperger syndrome. *Journal of Child psychology and Psychiatry* **38**, 813-822 (1997).

30 Bijsterbosch, J. D. *et al.* The relationship between spatial configuration and functional connectivity of brain regions. *Elife* **7**, e32992 (2018).

31 Gordon, E. M. *et al.* Precision functional mapping of individual human brains. *Neuron* **95**, 791-807. e797 (2017).

32 Van Essen, D. C. *et al.* The WU-Minn Human Connectome Project: an overview. *NeuroImage* **80**, 62-79, doi:10.1016/j.neuroimage.2013.05.041 (2013).

33 Van Essen, D. C. *et al.* The WU-Minn human connectome project: an overview. *Neuroimage* **80**, 62-79 (2013).

34 Bellec, P. *et al.* Impact of the resolution of brain parcels on connectome-wide association studies in fMRI. *Neuroimage* **123**, 212-228 (2015).

35 Van Essen, D. C., Glasser, M. F., Dierker, D. L., Harwell, J. & Coalson, T. Parcellations and hemispheric asymmetries of human cerebral cortex analyzed on surface-based atlases. *Cerebral cortex (New York, N.Y. : 1991)* **22**, 2241-2262, doi:10.1093/cercor/bhr291 (2012).

36 Nieuwenhuys, R. The myeloarchitectonic studies on the human cerebral cortex of the Vogt-Vogt school, and their significance for the interpretation of functional neuroimaging data. *Brain structure & function* **218**, 303-352, doi:10.1007/s00429-012-0460-z (2013).

37 Greene, A. S., Gao, S., Scheinost, D. & Constable, R. T. Task-induced brain state manipulation improves prediction of individual traits. *Nature communications* **9**, 2807 (2018).

38 Finn, E. S. *et al.* Functional connectome fingerprinting: identifying individuals using patterns of brain connectivity. *Nature neuroscience* (2015).

39 Gratton, C. *et al.* Functional brain networks are dominated by stable group and individual factors, not cognitive or daily variation. *Neuron* **98**, 439-452. e435 (2018).
40 Molnár, Z. in *Neural circuit development and function in the brain* 109-129 (Elsevier, 2013).
41 Mountcastle, V. B. Modality and topographic properties of single neurons of cat's somatic sensory cortex. *Journal of neurophysiology* **20**, 408-434, doi:10.1152/jn.1957.20.4.408 (1957).
42 Joshi, A. *et al.* Unified framework for development, deployment and robust testing of neuroimaging algorithms. *Neuroinformatics* **9**, 69-84 (2011).
43 Scheinost, D. *et al.* Alterations in anatomical covariance in the prematurely born. *Cerebral cortex* **27**, 534-543 (2015).
44 Satterthwaite, T. D. *et al.* An improved framework for confound regression and filtering for control of motion artifact in the preprocessing of resting-state functional connectivity data. *Neuroimage* **64**, 240-256 (2013).
45 Conley, M. I. *et al.* The racially diverse affective expression (RADIATE) face stimulus set. *Psychiatry research* (2018).
46 Cohen, A. O., Conley, M. I., Dellarco, D. V. & Casey, B. in *Society for Neuroscience.*
47 Barch, D. M. *et al.* Function in the human connectome: task-fMRI and individual differences in behavior. *Neuroimage* **80**, 169-189 (2013).
48 Speer, M. E., Bhanji, J. P. & Delgado, M. R. Savoring the past: positive memories evoke value representations in the striatum. *Neuron* **84**, 847-856 (2014).
49 May, J. C. *et al.* Event-related functional magnetic resonance imaging of reward-related brain circuitry in children and adolescents. *Biological psychiatry* **55**, 359-366 (2004).
50 Glass, L. Moire effect from random dots. *Nature* **223**, 578 (1969).
51 Uğurbil, K. *et al.* Pushing spatial and temporal resolution for functional and diffusion MRI in the Human Connectome Project. *Neuroimage* **80**, 80-104 (2013).
52 Smith, S. M. *et al.* Resting-state fMRI in the human connectome project. *Neuroimage* **80**, 144-168 (2013).
53 Glasser, M. F. *et al.* The minimal preprocessing pipelines for the Human Connectome Project. *Neuroimage* **80**, 105-124 (2013).
54 Gomes, R. & Krause, A. in *ICML.* 391-398.
55 Salehi, M., Karbasi, A., Shen, X., Scheinost, D. & Constable, R. T. An exemplar-based approach to individualized parcellation reveals the need for sex specific functional networks. *Neuroimage, Submitted* **142** (2017).
56 Minoux, M. in *Optimization Techniques* 234-243 (Springer, 1978).
57 Lacadie, C. M., Fulbright, R. K., Rajeevan, N., Constable, R. T. & Papademetris, X. More accurate Talairach coordinates for neuroimaging using non-linear registration. *Neuroimage* **42**, 717-725 (2008).
58 Thomas Yeo, B. *et al.* The organization of the human cerebral cortex estimated by intrinsic functional connectivity. *Journal of neurophysiology* **106**, 1125-1165 (2011).

Acknowledgments

This work was supported by NIH Grants R01 MH111424 (R.T.C.) and DARPA Young Faculty Award D16AP00046 (A.K.). Two publicly available data sets were used in this work. The first data set was provided by the Midnight Scan Club (MSC)[31] project, funded by NIH Grants NS088590, TR000448 (NUFD), MH104592 (DJG), and HD087011 (to the Intellectual and Developmental Disabilities Research Center at Washington University); the Jacobs Foundation (NUFD); the Child Neurology Foundation (NUFD); the McDonnell Center for Systems Neuroscience (NUFD, BLS); the Mallinckrodt Institute of Radiology (NUFD); the Hope Center for Neurological Disorders (NUFD, BLS, SEP); and Dart Neuroscience LLC. This data was obtained from the OpenfMRI database. Its accession number is ds000224. The second data set was provided by the Human Connectome Project, WU-Minn Consortium (Principal Investigators: David Van Essen and Kamil Ugurbil; 1U54MH091657) funded by the 16 NIH Institutes and Centers that support the NIH Blueprint for Neuroscience Research; and by the McDonnell Center for Systems Neuroscience at Washington University.

Author Contributions

M.S., A.K., D.S., and R.T.C. conceived and formulated the study. M.S. and A.K. developed the spatial-constrained exemplar-based submodular parcellation algorithm. M.S. performed the parcellation analysis and predictive modeling. A.S.G. designed the task-battery, collected, and preprocessed the primary data (RTC data set). M.S. preprocessed MSC data set. M.S. wrote the manuscript with contributions from R.T.C. and A.S.G. All other authors commented on the paper.